Applied Acoustics 249 (2026) 111311

Contents lists available at ScienceDirect

Applied Acoustics

journal homepage: www.elsevier.com/locate/apacoust

Integrated numerical and machine learning framework for the vibro-acoustic analysis of car doors

Emanuele Garofalo [a,b,*], Gioele Isacchi [a], Marco Olivieri [b], Michele Ebri [b], Francesco Ripamonti [a]

[a] Department of Mechanical Engineering, Politecnico di Milano, Milan (MI) 20156, Italy
[b] Ferrari S.p.A., Maranello (MO) 41053, Italy

ARTICLE INFO

Keywords:
Automotive acoustics
Structural–acoustic coupling
Data-driven acoustic modelling
Structural optimization
Acoustic field prediction
Loudspeaker–structure interaction

ABSTRACT

Sound quality in modern vehicles is strongly influenced by the acoustic environment inside the cabin, where the car door plays a central role as both a vibrating structure and the mounting point for loudspeakers. This work introduces a novel integrated framework for car door vibro-acoustic design that combines numerical simulation, experimental validation, and machine learning. A simplified yet modular car door prototype is developed to reproduce the main structural and acoustic features of a real door while allowing flexible boundary conditions. A finite element model (FEM) of the prototype is validated through dedicated experimental campaigns, and is employed to generate a dataset of different structural configurations and their corresponding acoustic responses. This dataset is then used to train a feed-forward neural network aiming at predicting the sound pressure level with high accuracy at a negligible computational cost in comparison to FEM simulations. The trained model is finally used to perform statistical analysis of the effects of different boundary conditions in the radiated sound pressure. By identifying practical design guidelines for the optimal stiffness distribution of a general car door, this work demonstrates the value of integrating physics-based simulations with data-driven approaches. The results achieved can effectively support the design of complex vibro-acoustic systems, opening the way for more efficient optimization strategies in automotive engineering.

1. Introduction

Nowadays, car cabin sound quality is increasingly recognized as a key factor in the automotive industry. Manufacturers pay close attention to all aspects of a vehicle's NVH characteristics [1], also studying the acoustic environment inside the car cabin, which has a strong influence both on the well-being of passengers and on the perceived quality of the vehicle [2,3]. Indeed, research efforts are invested in the improvement of the acoustic performance of the car cabin, considering the refinement of the cabin design and also improving the integration of the cockpit audio system [4,5]. Among the various components affecting the acoustic experience, the car door plays a central role being one of the largest vibrating elements and hosting loudspeakers, directly impacting the sound field within the cabin.

The design of a car door, and in particular the integration of a loudspeaker into its structure to ensure good vibro-acoustic performance, represents a particularly complex engineering challenge. For years, numerical simulations, ranging from simplified analytical models to detailed finite element simulations, have been used to help the component design stage [6]. Numerical analyses based on physical models can capture the structural and acoustic response of components with good accuracy, but they are often computationally demanding. Therefore, they cannot be always easily considered to support the acoustic improvement of car cabin systems, especially when many design alternatives must be considered. In literature, several works on the car door design have focused on simulating very specific conditions, such as the vibro-acoustic behaviour of doors during slamming events [7], in the generation of the acoustic field inside the cockpit [8–10] or, more specifically, simulating a single specific integration condition of a loudspeaker within the door [11]. While useful, these studies typically analyse a limited number of configurations and cannot easily be extended to large-scale optimisation tasks. In recent years, artificial intelligence has given a boost to the use of computer aided strategies during the design phases. Neural networks, for instance, have been applied to problems such as modelling the sound field generated by a vibrating structure, starting from experimental data [12,13]. These works have demonstrated the potential of data-driven methods, but their scope has so far remained quite narrow, most of the time applied to

* Corresponding author at: Department of Mechanical Engineering, Politecnico di Milano, Milan (MI) 20156, Italy.
E-mail address: emanuele.garofalo@polimi.it (E. Garofalo).

https://doi.org/10.1016/j.apacoust.2026.111311
Received 29 November 2025; Received in revised form 12 March 2026; Accepted 13 March 2026

a single, fixed structural configuration.

In this context, the present work proposes an integrated approach that combines the predictive capabilities of physics-based simulations with the flexibility of machine learning modelling to support the structural design optimization of a car door, with a special focus on its vibro-acoustic performance. Furthermore, the methodology proposed in this work is employed to highlight general design guidelines to support the acoustic-oriented design of automotive doors, focusing on the influence of local stiffness variations on the overall acoustic radiation.

To this end, a simplified yet highly configurable car door prototype, referred to as the CarDoor, having equivalent comparable geometrical and dynamical characteristics of a real car door component, is introduced. The prototype was specifically designed with modular panels and multiple potential fixing points to study a wide range of structural configurations. In order to study the interaction between the car door and the car audio system, the CarDoor is equipped with a woofer loudspeaker. The CarDoor can therefore investigate the effect of different boundary condition sets on the speaker's performance in terms of radiated sound pressure, panel vibrations, and cavity resonances. Unlike previous research, through the development of a modular structure capable of generating a large variability of cases, simulations validated by experiments, and a machine-learning model able to approximate FEM results at negligible computational cost, this work presents an optimization strategy that provides guidelines for the car door design based on arbitrary acoustic targets.

The proposed workflow begins with the development of a finite element model of the CarDoor. The model is employed to simulate the vibro-acoustic behaviour of the car door with different structural configurations changing the boundary conditions to obtain different stiffness distributions in the door panels, generating a dataset that links each CarDoor boundary condition layout to its corresponding radiated sound. The dataset is then used to train a neural network specifically designed to associate each configuration with the resulting sound pressure. Once trained, the network is used to perform statistical analysis on the effects of reinforcing some regions of the panels deriving at the same time general guidelines for vibroacoustic design strategies of a car door to obtain target acoustic effects.

The rest of the paper is organised as follows: Section II describes the development of the CarDoor numerical model, including the loudspeaker modelling approach adopted to simulate the woofer and the measurements conducted for its validation. Then, the creation of a dataset used to train the neural network by means of FEM simulations is discussed, together with the description of the neural network architecture and the evaluation of its accuracy and generalization performance. In Section III, the trained neural network is implemented to investigate the influence of the car door structural constraints on its vibro-acoustic performance. Section IV presents the main conclusions of the paper, also addressing future applications of the proposed methodology.

2. Materials, models and methods

This work investigates a methodology to support the acoustic-oriented design of car doors by establishing a link between design solutions and sound pressure generation. The case study focuses on a car door prototype illustrated in Fig. 1, named as CarDoor. This test rig is specifically conceived with a highly rigid frame with simplified geometries inspired by a car door, and it hosts a woofer loudspeaker. The prototype is designed to allow a modular setting of the boundary conditions of the front and rear panels, aiming to study the effects of the coupling between the woofer and the car door with their vibro-acoustic behaviour. The analysis is focused on the $30-200Hz$ frequency range, fully covering the typical operating bandwidth of the woofer loudspeaker.

The CarDoor, as illustrated in Fig. 2, features 68 potential fixing points,32 on the rear panel and 36 on the front panel. Each fixing point

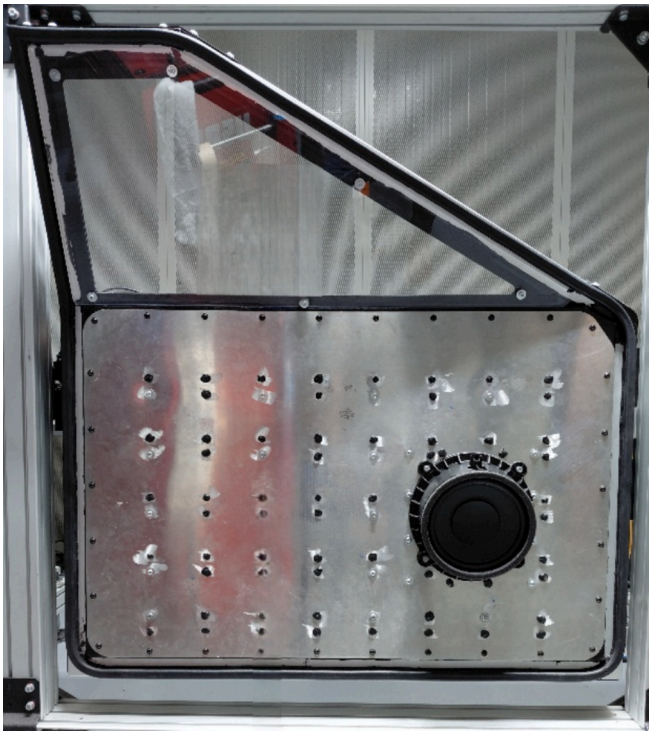

Fig. 1. CarDoor test rig.

can either be rigidly constrained to the internal supporting frame by means of a bolted metal-to-metal connection between the aluminium panel and the internal steel frame, with no compliant elements introduced in the joint, or left free to vibrate. This leads to a total of 2^{68} possible structural configurations, characterized by different constraining layouts of the car door panels. Under the assumption of linear system behaviour, the excitation from the woofer loudspeaker with the same input signal, each configuration produces a distinct vibro-acoustic response, resulting in up to 2^{68} different potential radiated sound fields.

The workflow proposed in this work, illustrated in Fig. 3, aims to enable a field-to-structure design approach, in which a desired acoustic field provides guidelines for determining the optimal structural configuration of an automotive door. To this end, based on the developed test rig, a numerical model of the system is built in COMSOL Multiphysics [14]. The model is optimized to achieve a trade-off between accuracy and computational efficiency, ensuring its suitability for subsequent optimization workflows. After being validated through experimental measurements, the numerical model is used to generate a dataset containing different fixing layouts of the car door together with their corresponding sound radiation. This dataset is then employed to train a neural network designed to associate each door configuration with its radiated sound field. The trained network is subsequently used to explore a wider range of configurations, enabling statistical analyses on the influence of each fixing point, identifying those that most significantly affect the system's sound radiation, and quantifying how each constraint contributes to either amplifying or attenuating the resulting sound pressure level (SPL).

2.1. Car door numerical model

To properly capture the vibro-acoustic behavior of the CarDoor, particular attention was first devoted to the modelling of the loudspeaker, which represents the excitation source of the system.

For years, researchers have approached dynamic loudspeaker modelling with varying levels of complexity, depending on the application type, main working frequency ranges, and simulation

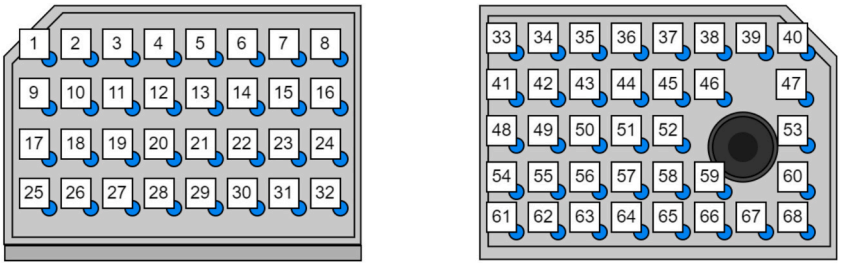

Fig. 2. Car door panel points that can be rigidly constrained to obtain a specific door configuration. On the left the rear panel, on the right the front panel with a classical woofer position.

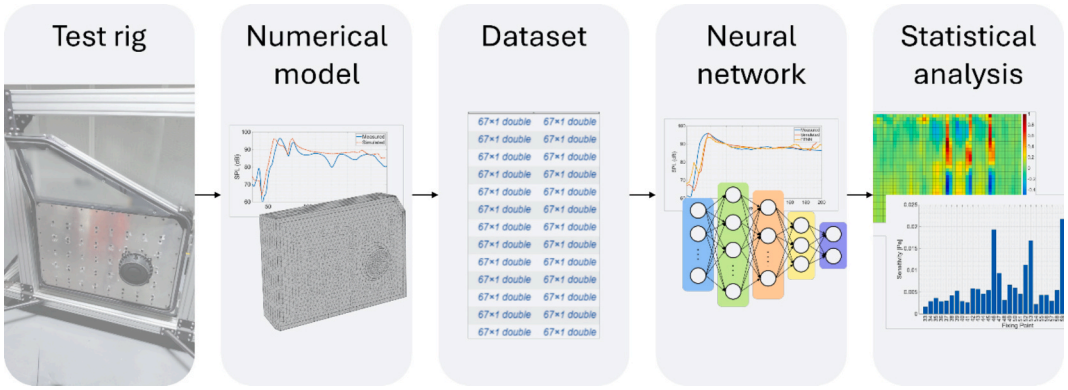

Fig. 3. Flow chart of the proposed methodology to obtain general guidelines for the design of the optimal structural configuration of an automotive door.

requirements. The distributed parameters approach is one of the most robust and comprehensive methods for simulating a dynamic loudspeaker. Based on the finite element method (FEM), it solves systems of partial derivative equations representing the electro-mechanical and acoustic behavior of the transducer. This approach is particularly well-suited for simulating local phenomena, system resonances, and non-uniformity of the device's electromagnetic field. Although this approach guarantees highly accurate results, it is computationally expensive and requires detailed computer-aided design (CAD) models and accurate knowledge of the materials used in order to correctly simulate their physical behaviour. For this reason, it is mainly implemented in applications and studies that focus exclusively on device design optimization. Modelling approaches based on experimental measurements are widely used alternatives. Measurements can indeed be used to synthetize loudspeaker models based on equivalent monopole sources replicating the device's sound radiation using acoustic transfer functions [15]. Experimental approaches can help to improve accuracy the of the simulations by alleviating problems related to possible distortion of the membrane [16] or generalizing the use of the equivalent source method for simulating the speaker mounted in any host structure [17]. One drawback of these methods is that extensive experimental campaigns focused exclusively on loudspeaker devices in specific environmental conditions, such as anechoic rooms, and mounted in dedicated test rigs with specific mounting layout are required to develop numerical models of loudspeakers for subsequent simulations. For this reason, their applicability is restricted to cases where a physical prototype of the loudspeaker is available making them not suitable for cases when the device has not yet been purchased, or when only its geometry and datasheet parameters are accessible, as in early design stages or virtual prototyping. In these scenarios, lumped parameter modelling approaches are more indicated. In literature, one of the most used formulations to model moving coil loudspeakers is the model based on the so-called Thiele-Small parameters [18–21]. Under the fundamental assumption of piston motion of the diaphragm, the model describes the physical behaviour of the device by solving equivalent electro-mechanical circuits shown in Fig. 4[22]:

In Fig. 4, the left-hand circuit represents the electrical domain of the transducer. Here, $\boldsymbol{V}$ denotes the input voltage source, $\boldsymbol{R_G}$ the generator resistance, $\boldsymbol{R_E}$ the voice coil resistance, while $\boldsymbol{L_E}(\boldsymbol{\omega})$ models the frequency-dependent voice coil inductance and $\boldsymbol{R_E}(\boldsymbol{\omega})$ accounts for magnetic losses. The values of $\boldsymbol{L_E}(\boldsymbol{\omega})$ and $\boldsymbol{R_E}(\boldsymbol{\omega})$ are computed according to the following equations:

$$\boldsymbol{L_E}(\boldsymbol{\omega}) = \frac{\boldsymbol{L_E^*}}{\boldsymbol{\omega}^{(\boldsymbol{n}-1)}\,\boldsymbol{sin}\left(\boldsymbol{n}\frac{\boldsymbol{\pi}}{\boldsymbol{2}}\right)} \tag{1}$$

$$\boldsymbol{R_E}(\boldsymbol{\omega}) = \frac{\boldsymbol{L_E^*}}{\boldsymbol{\omega}^{\boldsymbol{n}}\,\boldsymbol{cos}\left(\boldsymbol{n}\frac{\boldsymbol{\pi}}{\boldsymbol{2}}\right)} \tag{2}$$

where the value of $\boldsymbol{L_E^*}$ is derived from Equation (1) based on a reference value $\boldsymbol{L_E}(\boldsymbol{\omega_k})$, which is typically provided as a transducer parameter at a specific frequency $\boldsymbol{\omega_k}$. The term $\boldsymbol{n}$ denotes the voice coil loss factor. For standard moving coil loudspeakers, the parameter $\boldsymbol{n}$ typically assumes a value of 0.7[23].

The term $\boldsymbol{Bl}\cdot\boldsymbol{v}$ corresponds to the back electromotive force (EMF) induced when a coil of length $\boldsymbol{l}$ moves with velocity $\boldsymbol{v}$ in the magnetic field $\boldsymbol{B}$, and $\boldsymbol{i}$ is the current flowing through the coil. The right-hand circuit describes the mechanical domain, where the electromagnetic force $\boldsymbol{Bl}\cdot\boldsymbol{i}$ drives the diaphragm. The parameters $\boldsymbol{C_{MS}}$ and $\boldsymbol{R_{MS}}$ represent the suspension compliance and the mechanical damping, respectively, while $\boldsymbol{M_{MS}}$ denotes the effective moving mass of the system. Finally, the voltage source $\boldsymbol{F_D}$ models the acoustic load acting on the diaphragm surface $\boldsymbol{S_d}$.

In this work, for the loudspeaker simulation, the lumped-parameter model is adopted, since it combines ease of implementation, with practical accessibility since the required parameters have been provided in the manufacturer datasheets.

Before implementing the lumped-parameter model, the validity of the piston motion assumption of the loudspeaker diaphragm is assessed

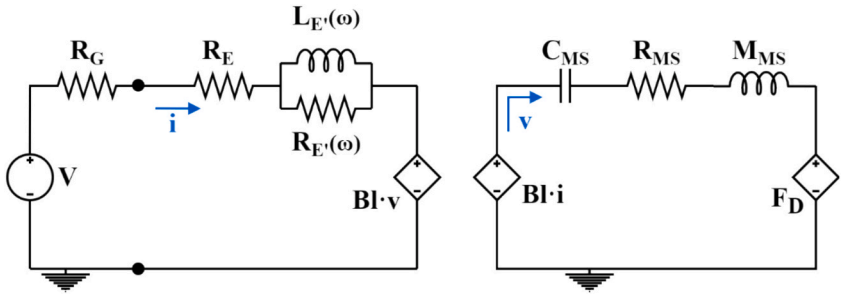

Fig. 4. Electro-mechanical equivalent circuit for simulating moving coil loudspeakers.

measuring the membrane velocity in several points (shown in Fig. 5a) using a laser doppler vibrometer (Polytec VibroGo VGO-200)[16], exciting the speaker with an exponential sine sweep signal from 30 Hz to 200 Hz at 1 W input power. Fig. 5b shows that all points on the loudspeaker diaphragm exhibit coherent normal vibration velocities, confirming that the speaker behaves as a rigid piston within the analyzed frequency range.

The CarDoor test rig has a geometry which represents a car door component, mounts a woofer loudspeaker and is composed of 2 mm aluminium front and rear panels with discrete points that can be rigidly constrained to an internal stiffening structure connected to the door frame. Furthermore, the entire door is rigidly mounted to a supporting structure, providing well-defined boundary conditions. This configuration allows selective fixation or relaxation of specific points to vary the vibro-acoustic response of the assembly.

Experimental measurements are conducted on the CarDoor to study its vibro-acoustic behaviour. The mechanical behaviour of the door panels is characterized through measurements of dynamic stiffness carried out at several points, shown in Fig. 6. Data acquisition is performed with the HEAD acoustics SQUADRIGA III system, employing PCB 356A03/NC accelerometers and a PCB 086C02 instrumented impact hammer.

Using the measured dynamic stiffness data, the damping factor ξ at each measurement point is estimated for each resonance frequency using the half-power bandwidth method [24]. Subsequently, the Rayleigh damping parameters α_i and β_i are calculated for each point. To obtain the final α and β values for each panel, the point-wise parameters are averaged across all measurement locations.

To optimize the COMSOL model in terms of computational efficiency, the door CAD model is simplified by removing geometric features that increase mesh complexity. Furthermore, components exhibiting minimal vibrational response to the woofer excitation, such as the window, the door frame, and the door support, are excluded from the analysis, allowing the model to focus exclusively on the car door cavity, with only the panels treated as flexible components. Preliminary tests confirmed that including these elements significantly increases simulation time without yielding a relevant improvement in model accuracy within the analyzed frequency range. Consequently, these simplifications are necessary to ensure the feasibility of generating the large-scale dataset required for training the neural network.

Considering the high stiffness ratio between the internal frame and the aluminium panels and the low-frequency range under analysis, the local compliance of the bolted joints can be considered negligible with respect to the global structural dynamics of the system. Accordingly, panel points that can either be rigidly attached to the internal stiffening structure or left free to vibrate are modelled as ideal fixed constraints when connected.

The acoustic domain in the FEM model explicitly encompasses both the external radiation space and the internal back cavity of the door. This approach enables the model to account for the acoustic loading on the panel as well as the acoustic impedance of the enclosure, which is represented by the voltage source F_D in the electro-mechanical circuit of Fig. 4. The value of F_D is computed according to Equation (3), where the term ΔP represents the pressure acting on the speaker.

$$F_D = \Delta P \cdot S_d; \tag{3}$$

The final COMSOL model combines the shell-based mechanical structure, the FEM acoustic pressure domain and the electrical circuit representation of the speaker described above, resulting in a coupled electro-vibro-acoustic model in which the system input is the voltage signal applied to the woofer.

All simulations are conducted assuming free-field conditions, with the floor modeled as an acoustically reflecting surface. To reduce the computational burden while preserving the relevant vibroacoustic in-

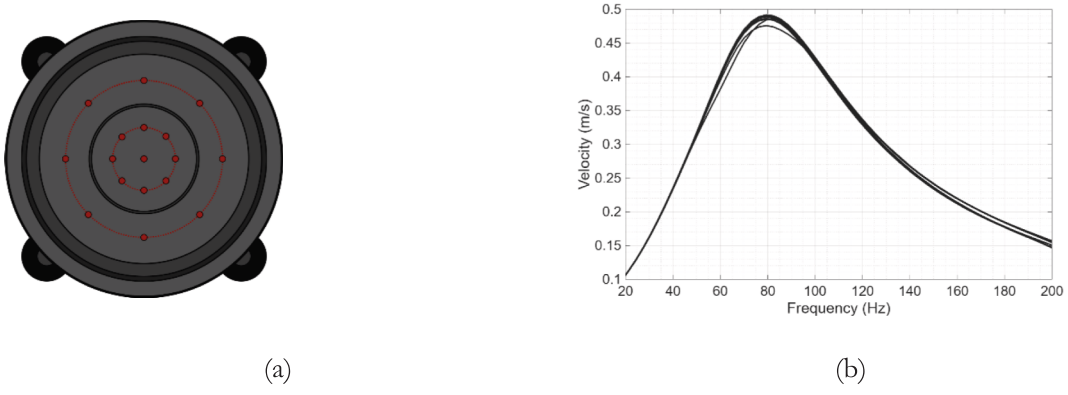

Fig. 5. Membrane velocity measurements for the validation of the diaphragm piston motion assumption: (a) measurement positions on the cone; (b) comparison of the membrane velocity measured at different positions.

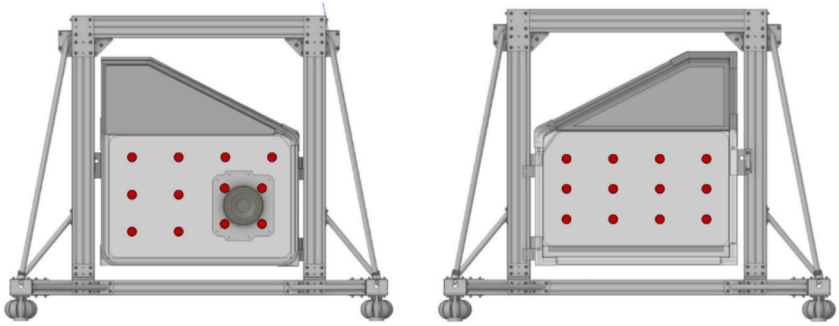

Fig. 6. Layout of measurement points for dynamic stiffness characterization.

formation, the simulations are restricted to the frequency range of 30–200 Hz, discretized with a resolution of 3 Hz. The model uses a mesh made of tetrahedral elements, whose maximum size is set to be less than one-fifth of the minimum wavelength.

3. Numerical model results

To validate the model, acoustic radiation measurements are performed on different door configurations by varying the fixing points of the panels. To minimize experimental uncertainties and ensure high repeatability, a microphone is positioned at a fixed distance of 0.5 m from the center of the front panel (Fig. 7). This setup was selected to facilitate a direct and reliable comparison between the numerical predictions and the experimental data, providing a controlled benchmark to assess the model's accuracy in capturing the radiated sound pressure level under different structural constraints. All measurements are conducted in an acoustically-treated environment to minimize room reflections.

Fig. 8 presents the results of the COMSOL model for three different door configurations, illustrating the comparison between measured and simulated sound pressure levels (SPL). Each subfigure displays both the SPL curves and a schematic representation of the points constrained in the model: blue markers denote points left free to vibrate, while red markers indicate points that are rigidly fixed. The comparison highlights how variations in the fixation points influence the vibrational behaviour of the panels and the resulting acoustic radiation, providing a clear validation of the model's ability to predict the sound field under different mechanical boundary conditions.

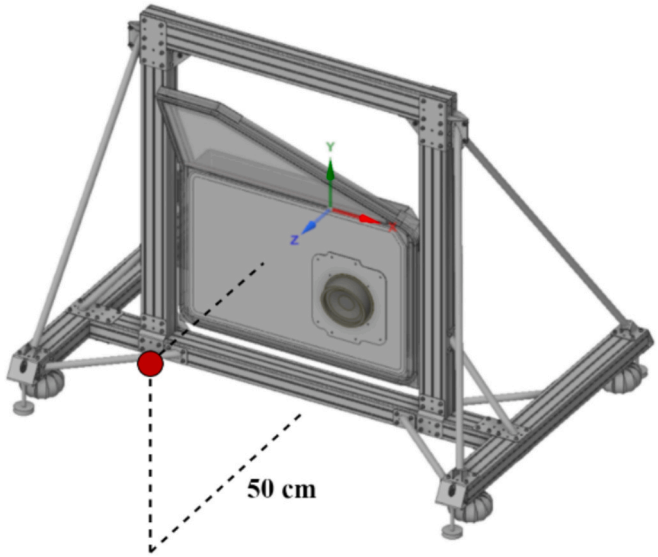

Fig. 7. Acoustic measurements layout for COMSOL model validation.

To further ensure the reliability of the numerical framework, structural vibrations are monitored using a PCB 356A03/NC accelerometer in the three layouts. The results, illustrated in Fig. 9, show the experimental data compared with FEM predictions in the 30–200 Hz range, expressed in terms of displacement normalized to the input voltage of the loudspeaker. The comparison for a representative accelerometer placed on the front panel (whose coordinates are reported in the figure) shows good agreement, confirming that the model accurately captures the vibrational field and the energy transmission to the panels.

All the simulations are carried out using a workstation mounting an Intel Core i7-14700 K processor, RAM of 64 Gb and using the COMSOL 6.3 software version. The average computation time required to evaluate a single door configuration is approximately 56 s. The combination of the model's accuracy and its computational efficiency generate large datasets containing information on both the door configurations and the resulting SPL within relatively short computation times.

3.1. Neural network design and validation

By labeling the potential fixing points of the panels, as illustrated in Fig. 2, and assigning to each point a Boolean variable (0 = *free*, 1 = *fixed*), each specific door configuration can be uniquely encoded by a binary code consisting of 68 digits.

To investigate the wide range of possible configurations, the Livelink interface between COMSOL Multiphysics and MATLAB is employed [25]. Multiple fixing layouts are automatically generated by random combinations of the binary codes, and the corresponding vibro-acoustic responses are simulated. This process results in the construction of a dataset that links each binary code to its associated SPL spectral curve, evaluated at the microphone position shown in Fig. 7. In total, 15000 distinct car door configurations are simulated and stored, requiring approximately 250hours of workstation computation time.

A machine learning approach is then employed to predict the acoustic response corresponding to a given structural configuration, uniquely identified by its binary code. The choice to design the network to receive a binary code as input and output the corresponding SPL spectrum stems from the goal of mapping a target acoustic response to an appropriate door configuration more efficiently than a classical FEM simulation. The task, formulated as a multivariate regression problem [26], is addressed by developing a fully connected feed-forward neural network (FFNN) [27,28] implemented with the MATLAB Deep Learning Toolbox [29]. The available dataset is subsequently split into a training set (70% of the total input–output pairs), a validation set (15%) and a test set (the remaining 15%), and Min-Max normalization is applied to the outputs to ensure a more stable convergence during training [30,31].

The design of the neural network architecture begins with an input layer the size of which corresponds to the dimensionality of the binary code representing the door configuration. This layer is followed by a sequence of fully connected hidden layers with 512, 256, 128, and 64 neurons, respectively. Each hidden layer is equipped with Batch Normalization to improve training stability [32], a rectified linear unit

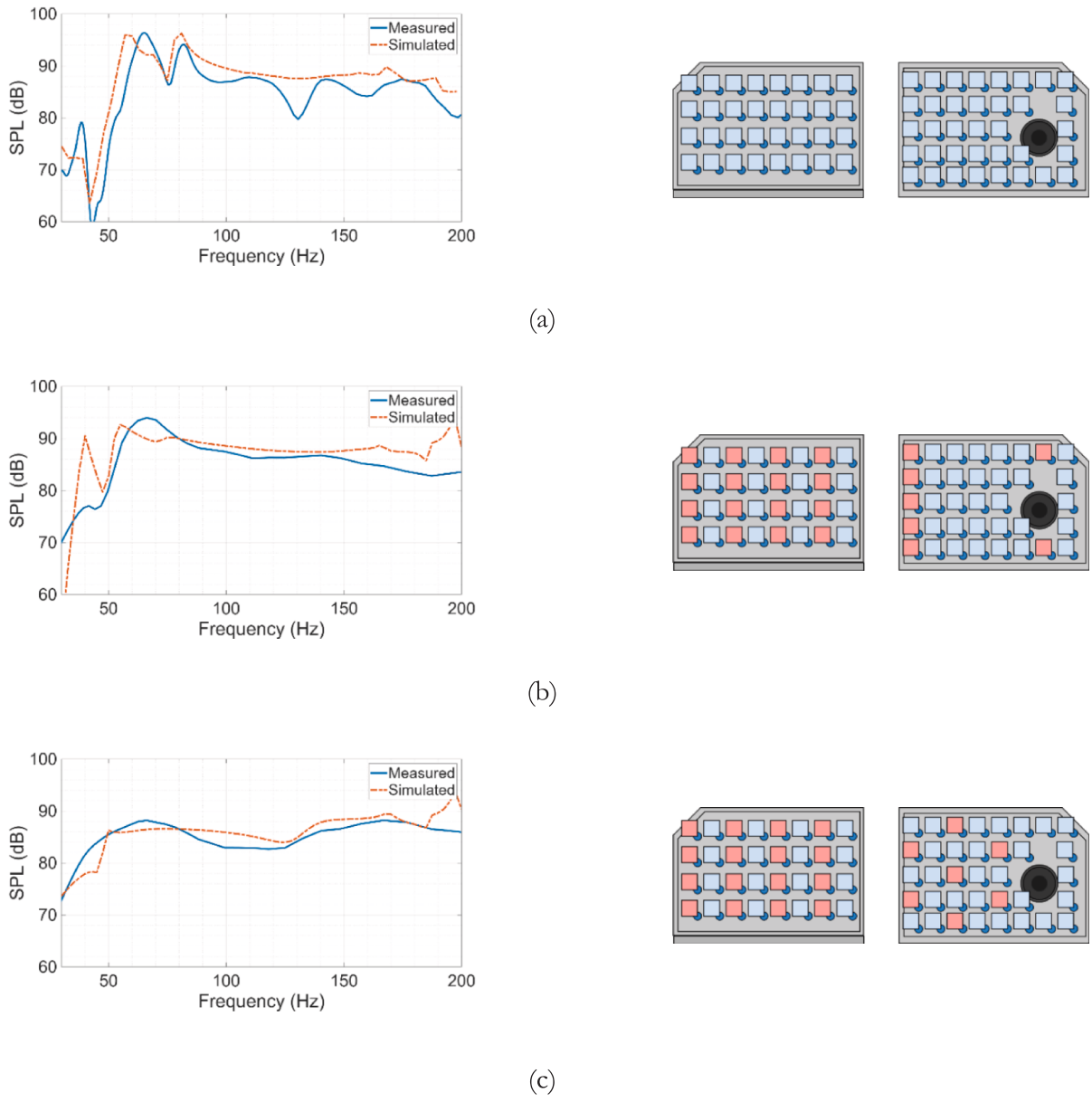

Fig. 8. Comparison between the SPL measured from the CarDoor and the SPL obtained from the COMSOL electro-vibro-acoustic model, considering different car door configurations.

(ReLU) activation function to introduce nonlinearity [33], and a dropout mechanism with a probability of 0.2 to reduce the risk of overfitting [34]. The final stage of the network is a linear output layer whose dimensionality matches the number of bins in the SPL spectrum to be predicted.

To evaluate the performance of the FFNN the metrics of the Root Mean Square Error (*RMSE*) (Equation (4), Mean Absolute Error (*MAE*) (Equation (5), and the coefficient of determination (R^2) (Equation (6) are used [35,36].

$$RMSE = \frac{1}{N_{conf} \cdot N_{freq}} \cdot \sqrt{\sum_{j=1}^{N_{freq}} \left(\sum_{i=1}^{N_{conf}} \left(Y(\omega_j) - \widehat{Y}(\omega_j) \right)^2 \right)} \tag{4}$$

$$MAE = \frac{1}{N_{conf} \cdot N_{freq}} \cdot \sum_{j=1}^{N_{freq}} \left(\sum_{i=1}^{N_{conf}} \left| Y(\omega_j) - \widehat{Y}(\omega_j) \right| \right); \tag{5}$$

$$SS_{res}(\omega_j) = \sum_{i=1}^{N_{conf}} \left(Y_i(\omega_j) - \widehat{Y}(\omega_j) \right)^2;$$

$$SS_{tot}(\omega_j) = \sum_{i=1}^{N_{conf}} \left(Y_i(\omega_j) - \frac{1}{n} \cdot \sum_{z=1}^{N_{conf}} Y_z(\omega_j) \right)^2; \tag{6}$$

$$R^2 = \frac{1}{N_{freq}} \cdot \sum_{j=1}^{N_{freq}} \left(1 - \frac{SS_{res}(\omega_j)}{SS_{tot}(\omega_j)} \right);$$

In the equations above the N_{conf} and N_{freq} represent respectively the total numbers of configurations present in the test dataset and the total number of frequency beams. The term $Y_i(\omega_j)$ is the absolute value of the SPL evaluated at the angular frequency ω_j generated by the i^{th} door configuration of the test set, and $\widehat{Y}_i(\omega_j)$ is the corresponding SPL value estimated by the neural network. The performance of the neural network is summarized in Table 1.

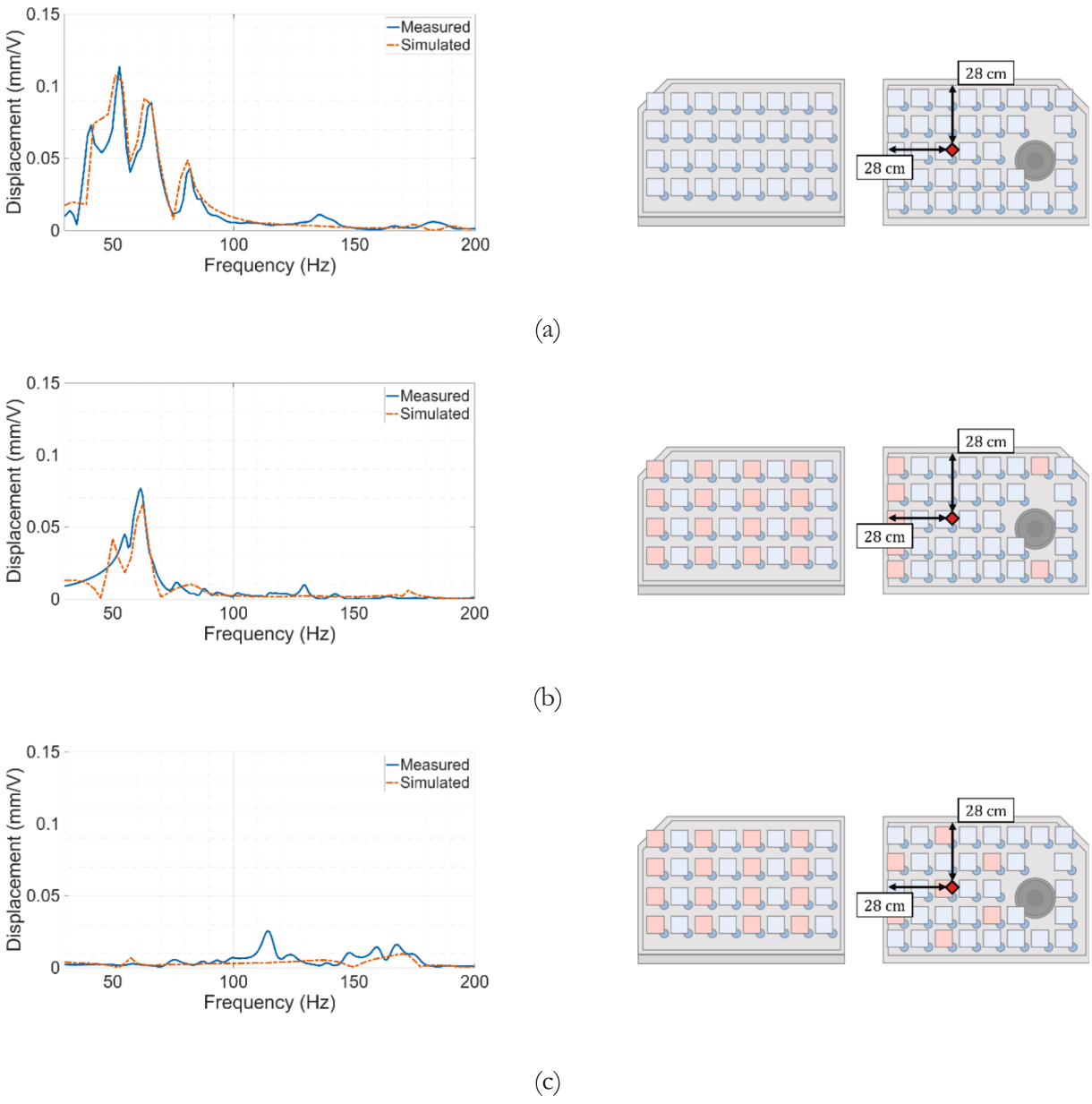

Fig. 9. Comparison between the structural vibrations measured from the CarDoor and the structural vibrations obtained from the COMSOL electro-vibro-acoustic model, considering different car door configurations.

Table 1
Neural network evaluation metrics results.

RMSE	0.025*Pa*
MAE	0.016*Pa*
R^2	0.7

In Fig. 10, three randomly selected curves from the FEM simulations of the test dataset are compared with the corresponding ones estimated by the network, showing that the model achieves an acceptable level of predictive accuracy, also considering the FFNN performance provided in Table 1. The network is able to reproduce the acoustic response with only minor deviations from the true values, demonstrating a strong overall correspondence between predicted and actual curves.

Although the agreement between FEM predictions, neural network estimates, and measurements is generally satisfactory within the main operating frequency band, a reduced correlation is observed above approximately 150 Hz. This behavior can be attributed to several physical and modelling aspects. At higher frequencies, the structural modal density of the panels increases significantly, making the system response more sensitive to local boundary conditions and joint compliance. In the present model, fixing points are idealized as perfectly rigid constraints, whereas real connections exhibit finite stiffness and localized damping effects. Moreover, higher-order panel modes become more spatially complex and may require a finer mesh resolution for full accuracy. For these reasons, the combined influence of these modelling simplifications becomes more evident above 150 Hz. Nevertheless, as these frequencies fall outside the operating range of the woofer, the modelling assumptions and mesh refinement were specifically optimized for the functional bandwidth.

4. Vibro-acoustic analysis

The intrinsic efficiency of the trained FFNN is implemented to investigate the influence of the local constraints of the CarDoor system on its vibro-acoustic performance. Random combinations of fixing

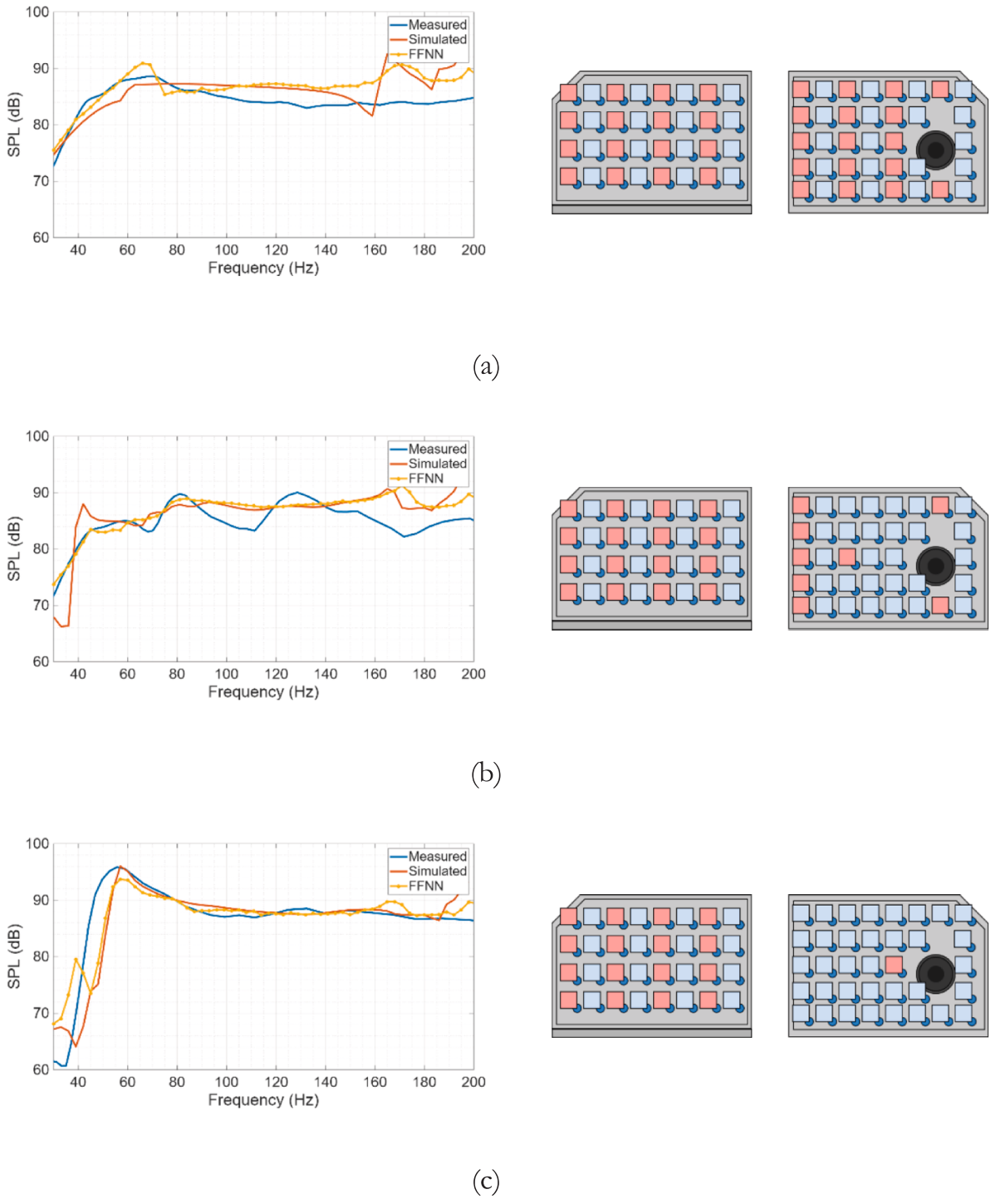

Fig. 10. Comparison between the SPL estimated form the FFNN, the correspondent SPL from the FEM model of the CarDoor test rig, and the measurements, considering cases belonging to the test set of the Dataset.

layouts are generated to reproduce the variability typically observed in real automotive doors, whose panels are characterized by non-homogeneous mechanical properties across different regions. This statistical approach enables the identification of global trends and macro-scale vibro-acoustic behaviours associated with the stiffening or relaxation of specific areas, providing a broader understanding of how structural modifications influence the system acoustic radiation.

To assess the influence of each potential fixing point on the overall acoustic response, a sensitivity analysis is carried out using the trained neural network. Starting from a set of 10^5 randomly generated structural configurations, each defined by a binary vector indicating the state (fixed or free) of the 68 available points, an iterative inversion of the state of one fixing point at a time is introduced, keeping all other fixing points unchanged. As indicated in Equation (7), for each inversion, the variation in the predicted sound pressure across all frequencies and configurations is evaluated. This way, the average absolute variation can be quantified to assess the sensitivity of the system vibro-acoustic performance to each fixing point.

$$sens_i = \frac{1}{N_{conf}} \cdot \frac{1}{N_{freq}} \cdot \left(\sum_{j=1}^{N_{conf}} \left(\sum_{z=1}^{N_{freq}} \left| p_{j_{original}}(\omega_z) - p_{j_i}(\omega_z) \right| \right) \right); \quad (7)$$

In Equation (7), $sens_i$ indicates the sensitivity of the i^{th} fixing point, N_{conf} is the number of random configurations estimated by the network, N_{freq} is the number of the analyzed frequencies. The term $p_{j_{original}}(\omega_z)$ is the modulus of the sound pressure generated by the j^{th} door configuration in its original configuration evaluated at the angular frequency ω_z while $p_{j_i}(\omega_z)$ is the modulus of the sound pressure generated by the same configuration with the state of the i^{th} point inverted.

The results, shown in Fig. 11, highlight the impact of each constraint on the door's vibro-acoustic behavior.

The sensitivity analysis reveals that the fixing points located in the proximity of the loudspeaker mounting area exhibit the highest influence on the predicted SPL. This result highlights that the mechanical constraint conditions around the loudspeaker strongly influence the overall acoustic radiation by directly modifying the coupling between the panel vibration and the acoustic field. Other regions showing significant sensitivity are those located farther from the door frame, where local boundary condition variations substantially alter the panel deformation patterns, thereby affecting the acoustic radiation of the door.

To further quantify the correlation between the fixing points layout and the vibro-acoustic response of the CarDoor, a statistical analysis is carried out by analyzing the 10^5 configurations estimated by the network. For each 1/6-octave frequency band b and fixing point i, the difference in fixing probability between configurations whose SPL is above and below the mean value is computed as Equation (8):

$$\Delta P_{i_{fix}}(b) = P^{above}_{i_{fix}}(b) - P^{below}_{i_{fix}}(b) \quad (8)$$

Where $P^{above}_{i_{fix}}(b)$ and $P^{below}_{i_{fix}}(b)$ are the fractions of configurations in which point i is fixed among those with SPL respectively above (A_b) and below (B_b) the mean SPL of the frequency band b.

$$P^{above}_{i_{fix}}(b) = \frac{1}{|A_b|} \cdot \sum_{j \in A_b} X_{ij} \quad (9)$$

$$P^{below}_{i_{fix}}(b) = \frac{1}{|B_b|} \cdot \sum_{j \in B_b} X_{ij} \quad (10)$$

In Equation (9) and Equation (10), $|A_b|$ and $|B_b|$ are the number of configurations generating a SPL above and below the mean SPL computed in the frequency band b while X_{ij} is binary variable representing the state of the fixing point i ($X = 1 \rightarrow fixed$, $X = 0 \rightarrow free$). A positive value of $\Delta P_{i_{fix}}$ indicates that the fixing of the i^{th} point tends to increase the SPL in the b^{th} frequency band, whereas negative values indicate a reduction effect.

The results of the analysis are reported in Fig. 12, highlighting the frequency-dependent structural–acoustic interactions through a heat-map representation of the probability ΔP. In the plot, positive values (red cells) indicate that fixing the corresponding point tends to increase the SPL and negative values (blue cells) indicate that fixing the point tends to reduce the SPL.

The results illustrate that by fixing the points close to the speaker diaphragm, a reduction in the lower frequency bands can be observed, while the acoustic radiation of higher frequency bands is amplified.

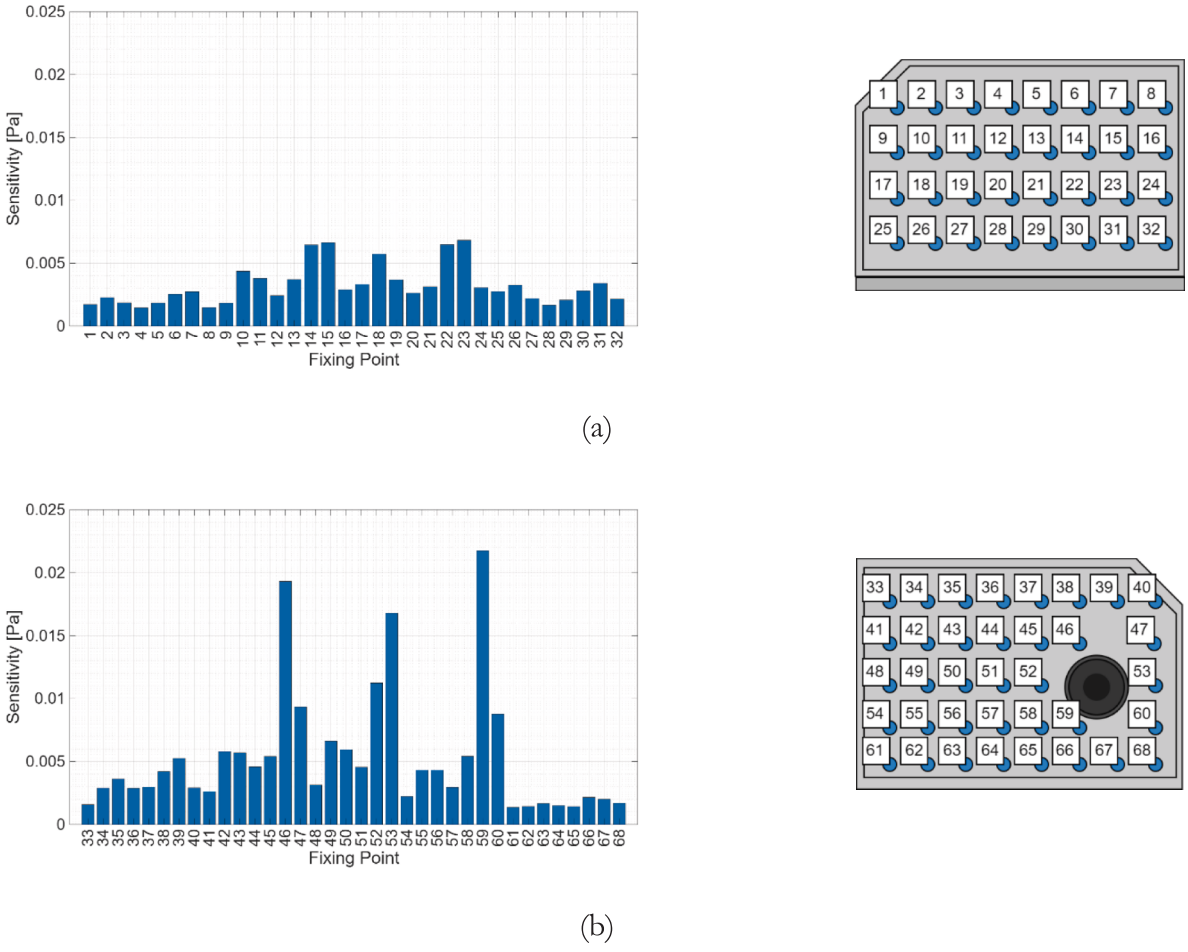

Fig. 11. Comparison of the sensitivity of the CarDoor vibro-acoustic response to the layout of the fixing points of the rear panel (b) and front panel (a).

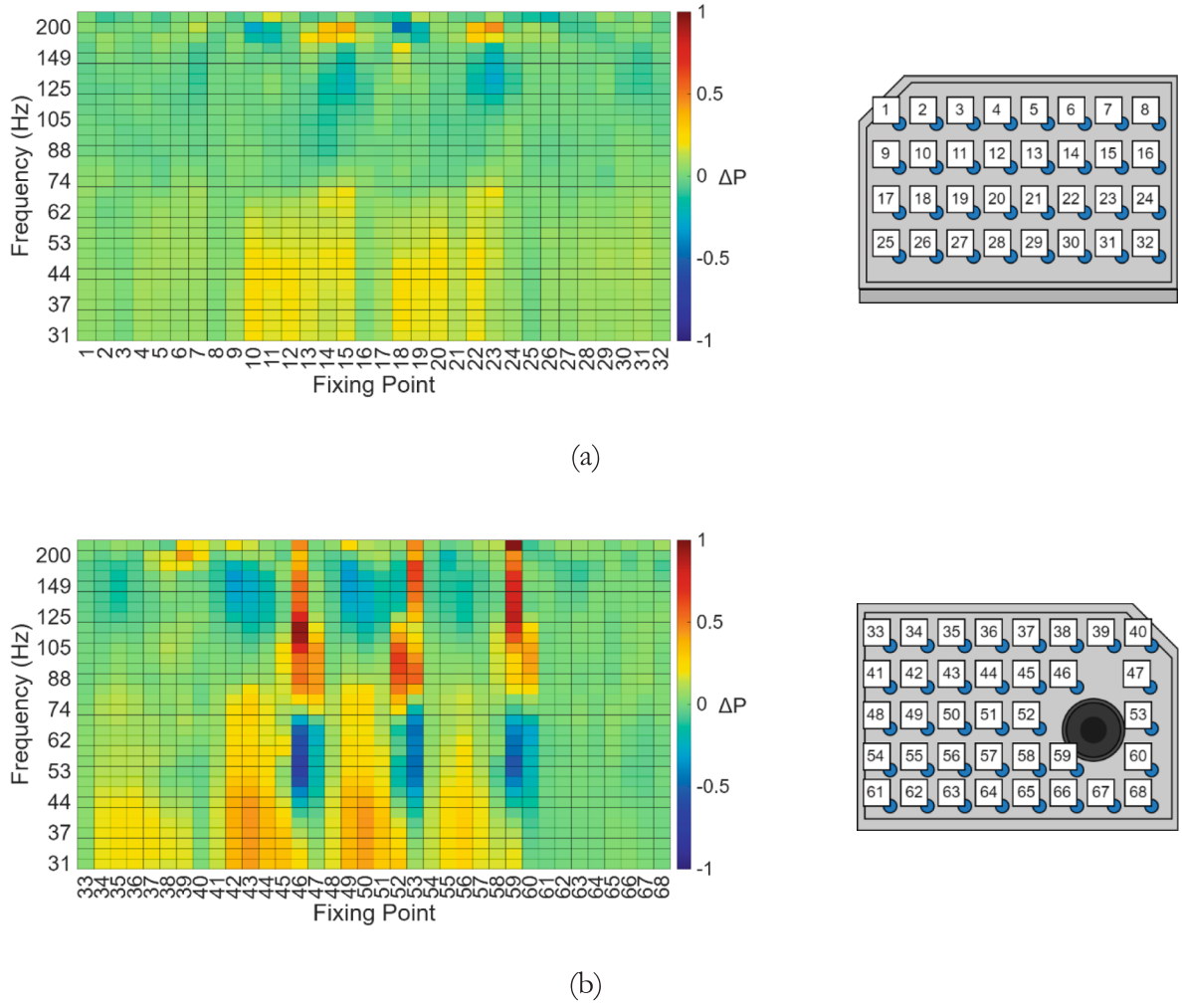

Fig. 12. Influence of fixing points layout on the radiated SPL, (a) frontal panel and (b) rear panel.

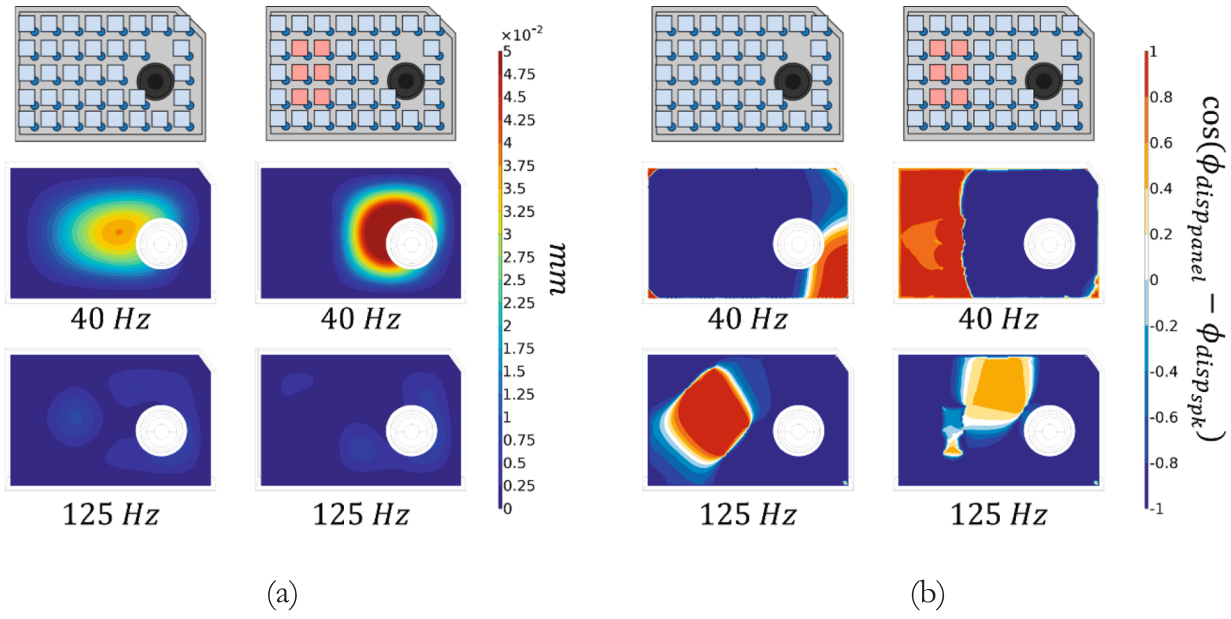

Fig. 13. Comparison between the unconstrained and central fixing points panel configurations. (a) Displacement field of the panel. (b) Cosine of the phase difference between the panel displacement and the loudspeaker diaphragm displacement at 40 Hz and 125 Hz.

Indeed, constraining the central points of the panels statistically tends to amplify the SPL at lower frequency bands and reduce the radiated pressure at higher frequencies.

The influence of panel constraints on the radiated SPL can be understood by considering the panel as a secondary acoustic source coupled with the loudspeaker diaphragm. Depending on the constraint layout, portions of the panel may vibrate in phase or out of phase with the diaphragm, either reinforcing or reducing the radiated sound. It should be noted that the results reported in this study are based on a statistical analysis over multiple configurations; therefore, the response of a single configuration may not fully reflect the overall trend. To provide a clearer physical interpretation, three representative configurations are analyzed (central constraints, constraints at the woofer attachment points, and an unconstrained panel) by examining the panel displacement field and the cosine of the difference between the phase of the panel displacement ($\phi_{disp_{panel}}$) and the phase of the diaphragm displacement ($\phi_{disp_{spk}}$) at selected frequencies. The displacement magnitude plots indicate the modal deformation patterns of the panel, while the phase plots show whether each panel region vibrates in phase with the loudspeaker $\left(\cos\left(\phi_{disp_{panel}} - \phi_{disp_{spk}}\right) \approx 1\right)$ or in counterphase $\left(\cos\left(\phi_{disp_{panel}} - \phi_{disp_{spk}}\right) \approx -1\right)$.

The results, reported in Fig. 13, illustrate the physical mechanisms responsible for the SPL variations induced by fixing the central points of the panel. In particular, at 40 Hz and 125 Hz, where amplification and attenuation of the radiated SPL are respectively observed, the analysis clarifies how the constraint-induced modification of the modal shape and phase distribution affects the constructive or destructive interference between the panel and the loudspeaker radiation.

At 40 Hz, constraining the central region concentrates the panel vibrations around the woofer and significantly reduces regions vibrating in counterphase with the diaphragm. This reduction in out-of-phase radiation weakens destructive interference, leading to an overall increase in the radiated SPL. In contrast, at 125 Hz, the same constraints strongly suppress the in-phase vibration of the panel, diminishing the constructive contribution to the acoustic field and reducing the radiated SPL.

The results, reported in Fig. 14, illustrate the physical mechanisms associated with constraining the panel near the woofer attachment points. In particular, at 60 Hz and 100 Hz, where attenuation and amplification of the radiated SPL are respectively observed.

As shown by the results, applying constraints near the woofer leads to a reduction of the radiated SPL at 60 Hz. This behavior is associated with the fact that, in this configuration, the panel predominantly vibrates in counterphase with respect to the woofer diaphragm, thereby promoting destructive interference. Conversely, at 100 Hz, the observed increase in SPL can be attributed to larger portions of the panel vibrating in phase with the woofer, which enhances constructive interference in the radiated acoustic field compared to the unconstrained case.

It is important to note that a reduction in the radiated SPL caused by the fixation of certain panel regions should not be interpreted solely as a negative effect. In some frequency ranges, increased stiffness may lead to a reduction of panel vibrations and, consequently, of internal reverberation phenomena. This behaviour can result in a clearer and more controlled low-frequency response, ultimately improving the perceived acoustic quality.

Overall, these results show that the proposed methodology effectively supports the acoustics-driven design of automotive car doors by identifying the panel regions that most influence acoustic radiation and by enabling a physically grounded interpretation of the effects induced by their stiffening. By combining numerical modelling, experimental validation, and data-driven predictions, the approach provides a robust decision-support tool that guides early-stage design, informs optimization processes, and ultimately contributes to the development of automotive components with improved and more predictable acoustic performance.

5. Conclusions

This work presents a methodology to support the acoustic-oriented design of car doors, combining finite element simulations, experimental validation, and machine learning. A modular car door prototype (CarDoor) is developed to reproduce the main structural and acoustic features of real components by allowing variable boundary conditions' layouts. The finite element model, validated against measurements, is implemented to generate a large dataset of structural configurations, which is used to train a feed-forward neural network capable of accurately predicting the radiated sound pressure level with minimal computational cost compared with FEM simulations.

The trained model proved to be effective for statistical and sensitivity analyses, identifying the structural regions that most influence the

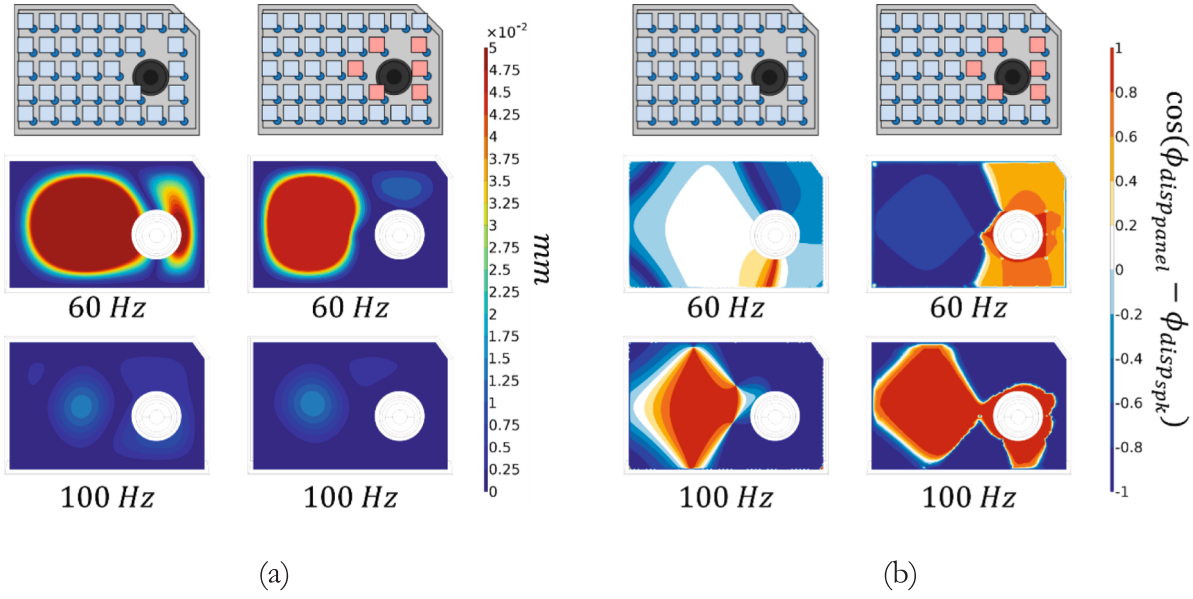

Fig. 14. Comparison between the unconstrained panel and the panel with fixing points close to the woofer. (a) Displacement field of the panel. (b) Cosine of the phase difference between the panel displacement and the loudspeaker diaphragm displacement at 60 Hz and 100 Hz.

acoustic response. Results show that fixing specific panel areas can either amplify or attenuate selected frequency bands, depending on the induced stiffness distribution.

To respect the generality of the methodology, the validation is performed on a simplified prototype under controlled conditions. However, the current model is still limited by the assumption of linear behaviour, neglecting nonlinear phenomena such as rattles, assembly gaps, and loudspeaker distortions. Furthermore, the model's accuracy, particularly at higher frequencies, relies on idealized assumptions such as the perfect rigidity of the fixing points. This limitation could be addressed in future research by conducting targeted experimental campaigns to characterize the actual mechanical impedance of the joints, allowing for a more refined calibration of the FEM model through the use of discrete spring-damper elements.

Future research will focus on extending the proposed methodology to more complex and representative door architectures, exploring diverse loudspeaker types and mounting configurations. Additionally, the framework will be evolved to incorporate physical parameters such as panel thickness and material properties as input features, enabling the model to predict how structural variations impact the radiated acoustic response. Furthermore, future developments will extend the methodology to a multi-point acoustic grid, further validating the network's accuracy in predicting the spatial distribution of the sound field.

Finally, the scalability of this approach will be validated by integrating the door model into a full cockpit environment to assess its performance in a complete vehicle system.

These developments aim to consolidate the proposed framework into a reliable and versatile tool for early-stage design and optimization of complex automotive vibro-acoustic systems.

CRediT authorship contribution statement

Emanuele Garofalo: Writing – review & editing, Writing – original draft, Validation, Software, Methodology, Formal analysis, Data curation, Conceptualization. **Gioele Isacchi:** Writing – review & editing, Methodology, Conceptualization. **Marco Olivieri:** Writing – review & editing, Methodology, Conceptualization. **Michele Ebri:** Supervision, Project administration, Conceptualization. **Francesco Ripamonti:** Supervision, Project administration.

Declaration of competing interest

The authors declare that they have no known competing financial interests or personal relationships that could have appeared to influence the work reported in this paper.

Acknowledgments

This study is part of a research project involving Politecnico di Milano and Ferrari S.p.A. The authors gratefully acknowledge Ferrari S.p.A. for providing the support and data necessary for this work.

Data availability

Data will be made available on request.

References

[1] R. Citarella et al., 'Structural and Vibro-Acoustics Optimization of a Car Body Rear Part', Appl. Sci., vol. 13, no. 6, Art. no. 6, Jan. 2023, doi: 10.3390/app13063552.
[2] Bezat M-C, Kronland-Martinet R, Roussarie V, Ystad S. From acoustic descriptors to evoked quality of car door sounds. J Acoust Soc Am Jul. 2014;136(1):226–41. https://doi.org/10.1121/1.4883364.
[3] Botti T, Olivieri M, Gino J, Oliva A. Enhancing in-vehicle speech intelligibility: a study on the benefits of active Road Noise Cancellation system. presented at the Forum Acusticum Euronoise 2025. 2025.
[4] 'AES Convention Papers Forum » Automotive Audio Design (A Tutorial)'. Accessed: Jun. 23, 2025. [Online]. Available: https://secure.aes.org/forum/pubs/conventions/?elib=9062.
[5] Liao X, Cheer J, Elliott SJ, Zheng S. Design of a Loudspeaker Array for Personal Audio in a Car Cabin. J Audio Eng Soc 2017;65(3):Mar.
[6] H. S. Hussein, 'Numerical Study of Automotive Doors', Aug. 2012, Accessed: Jun. 20, 2025. [Online]. Available: https://www.academia.edu/66350715/Numerical_Study_of_Automotive_Doors.
[7] C. A. Niccolini Marmont Du Haut Champ and P. Silvestri, 'Experimental and numerical vibro-acoustic investigation on a trimmed car door to analyze slamming event', Appl. Acoust., vol. 166, p. 107380, Sep. 2020, doi: 10.1016/j.apacoust.2020.107380.
[8] Montrasio M, Ripamonti F. A multi-channel active noise control logic for reducing airborne noise transmission through an open car window. JVCJournal Vib Control 2025. https://doi.org/10.1177/10775463251362261.
[9] Aretz M, Vorländer M. Combined wave and ray based room acoustic simulations of audio systems in car passenger compartments, Part I: Boundary and source data. Appl Acoust Feb. 2014;76:82–99. https://doi.org/10.1016/j.apacoust.2013.07.021.
[10] Garofalo E, et al. Identification of acoustic characteristic of tweeter loudspeakers for car cabin sound quality simulations. Forum Acusticum Euronoise 2025, 2025..
[11] D. Lennström, 'In-Situ Characterization of Vibrations from a Door Mounted Loudspeaker', SAE International, Warrendale, PA, SAE Technical Paper 2018-01–1511, Jun. 2018. doi: 10.4271/2018-01-1511.
[12] Wang YS, Lee C-M, Kim D-G, Xu Y. Sound-quality prediction for nonstationary vehicle interior noise based on wavelet pre-processing neural network model. J Sound Vib Feb. 2007;299(4):933–47. https://doi.org/10.1016/j.jsv.2006.07.034.
[13] Wang YS, Guo H, Feng TP, Ju J, Wang XL. Acoustic behavior prediction for low-frequency sound quality based on finite element method and artificial neural network. Appl Acoust Jul. 2017;122:62–71. https://doi.org/10.1016/j.apacoust.2017.02.009.
[14] COMSOL Multiphysics. [Online]. Available: https://www.comsol.it/.
[15] Wang S, Li H, Zhang P, Tao J, Zou H, Qiu X. An experimental study on the upper limit frequency of global active noise control in car cabins. Mech Syst Sig Process Oct. 2023;201:110672. https://doi.org/10.1016/j.ymssp.2023.110672.
[16] E. Garofalo, G. Isacchi, S. Talucci, M. Ebri, A. Oliva, F. Ripamonti, 'Experimental analysis of a car loudspeaker model based on imposed vibration velocity: effect of membrane discretization', presented at the AES 157th Convention, New York, NY, USA: AES, 10/10 2024.
[17] Garofalo E, Isacchi G, Talucci S, Ebri M, Oliva A, Ripamonti F. Numerical modelling of a loudspeaker sound radiation and its dynamic interaction with the host structure. J Acoust Soc Am Aug. 2025;158(2):1344–54. https://doi.org/10.1121/10.0039064.
[18] Thiele, A Neville, 'Loudspeakers in vented boxes: part I', J. Audio Eng. Soc., vol. 19, no. 5, pp. 382–392, May 1971.
[19] Thiele A. Neville, 'Loudspeakers in vented boxes: Part II'. J Audio Eng Soc 1971;19(6):471–83.
[20] Small RH. Vented-box loudspeaker systems-part 1: small-signal analysis. J Audio Eng Soc Jun. 1973;21(5):363–72.
[21] Small RH. Vented-box loudspeaker systems-part 2: large-signal analysis. J Audio Eng Soc Aug. 1973;21(6):438–44.
[22] Sagers JD, Leishman TW, Blotter JD. An extended lumped-element model and parameter estimation technique to predict loudspeaker responses with possible surround-dip effects. J Acoust Soc Am Nov. 2013;134(5):3580–93. https://doi.org/10.1121/1.4820886.
[23] W. M. Leach, 'Loudspeaker Voice-Coil Inductance Losses: Circuit Models, Parameter Estimation, and Effect on Frequency Response'.
[24] Diana G, Cheli F. Dinamica dei sistemi meccanici. Polipress 2010.
[25] 'COMSOL Multiphysics Reference Manual'.
[26] Katipamula S, Reddy TA, Claridge DE. Multivariate Regression Modeling. J Sol Energy Eng Aug. 1998;120(3):177–84. https://doi.org/10.1115/1.2888067.
[27] Gao M, Liao T, Lu Y. Fully connected feedforward neural networks based CSI feedback algorithm. China Commun Jan. 2021;18(1):43–8. https://doi.org/10.23919/JCC.2021.01.004.
[28] Bebis G, Georgiopoulos M. Feed-forward neural networks. IEEE Potentials Oct. 1994;13(4):27–31. https://doi.org/10.1109/45.329294.
[29] 'Deep Learning Toolbox Documentation'. Accessed: Sep. 01, 2025. [Online]. Available: https://it.mathworks.com/help/deeplearning/index.html.
[30] Wu S, et al. L1 -Norm batch Normalization for Efficient Training of Deep Neural Networks. IEEE Trans Neural Netw Learn Syst Jul. 2019;30(7):2043–51. https://doi.org/10.1109/TNNLS.2018.2876179.
[31] L. Huang, J. Qin, Y. Zhou, F. Zhu, L. Liu, and L. Shao, 'Normalization Techniques in Training DNNs: Methodology, Analysis and Application', Sep. 27, 2020, arXiv: arXiv:2009.12836. doi: 10.48550/arXiv.2009.12836.
[32] V. Thakkar, S. Tewary, and C. Chakraborty, 'Batch Normalization in Convolutional Neural Networks — A comparative study with CIFAR-10 data', in 2018 Fifth International Conference on Emerging Applications of Information Technology (EAIT), Jan. 2018, pp. 1–5. doi: 10.1109/EAIT.2018.8470438.
[33] C. Banerjee, T. Mukherjee, and E. Pasiliao, 'An Empirical Study on Generalizations of the ReLU Activation Function', in Proceedings of the 2019 ACM Southeast Conference, in ACMSE '19. New York, NY, USA: Association for Computing Machinery, Apr. 2019, pp. 164–167. doi: 10.1145/3299815.3314450.

[34] Baldi P, Sadowski P. The dropout learning algorithm. Artif Intell May 2014;210: 78–122. https://doi.org/10.1016/j.artint.2014.02.004.
[35] V. Plevris, G. Solorzano, N. P. Bakas, and M. E. A. Ben Seghier, 'Investigation of performance metrics in regression analysis and machine learning-based prediction models', 2022.
[36] Tatachar, Abhishek V, 'Comparative assessment of regression models based on model evaluation metrics', Int. Res. J. Eng. Technol. IRJET, vol. 08, no. 09, 2021.